RESEARCH ARTICLE
doi: 10.2306/scienceasia1513-1874.2024.s002

ScienceAsia 50S (1): 2024: ID 2024s002: **1–11**

Tunable organosulfonic acid-functionalized natural rubber/wormhole-like mesostructured silica nanocomposites for enhancing the esterification of carboxylic acids with methanol

Krongkiat Na Lumphoon[a], Sukunya Ngampradit[a], Satit Yousatit[b], Toshiyuki Yokoi[c], Chawalit Ngamcharussrivichai[b,d,e], Sakdinun Nuntang[a,*]

[a] Industrial Chemistry Innovation Programme, Faculty of Science, Maejo University, Chiang Mai 50290 Thailand
[b] Department of Chemical Technology, Faculty of Science, Chulalongkorn University, Bangkok 10330 Thailand
[c] Chemical Resources Laboratory, Tokyo Institute of Technology, Yokohama 226-8503 Japan
[d] Center of Excellence on Petrochemical and Materials Technology (PETROMAT), Chulalongkorn University, Bangkok 10330 Thailand
[e] Center of Excellence in Catalysis for Bioenergy and Renewable Chemicals (CBRC), Faculty of Science, Chulalongkorn University, Bangkok 10330 Thailand

[*]Corresponding author, e-mail: Sakdinun.nt@gmail.com

Received 3 Feb 2024, Accepted 24 Sep 2024
Available online 10 Nov 2024

ABSTRACT: Organosulfonic acid-functionalized natural rubber/wormhole-like mesostructured silica (NR/WMS–SO_3H) nanocomposites, which are solid acid catalysts, are used in esterification due to their extensive surface area, shape-selective characteristics, extremely acidic sites, and hydrophobic behavior. Herein, NR/WMS–SO_3H catalysts with different mesoporosity and acidity values were synthesized via an in-situ sol–gel technique, in which tetraethylorthosilicate mixed with different primary amines ($C_nH_{2n+1}NH_2$, $n = 12$, 14, and 16) as structural templating agents were simultaneously condensed with 3-mercaptopropyl trimethoxysilane in an NR colloidal solution, followed by oxidation with hydrogen peroxide. The X-ray diffraction analysis and transmission electron microscopy revealed a wormhole-like framework of the NR/WMS–SO_3H composites. The use of amine templates with longer alkyl chains provided the NR/WMS–SO_3H catalysts with a larger pore diameter, acidity, and enhanced hydrophobic properties. This study exhibited the development and production of customized acidic hybrid mesoporous silica catalysts with specific characteristics such as mesoporosity, acidity, and hydrophobicity. Moreover, the NR/WMS–SO_3H catalysts demonstrated improved catalytic efficacy in comparison to regular organosulfonic acid–functionalized wormhole-like mesostructured silica in the esterification of acetic, octanoic, and palmitic acids with methanol. The hydrophobic properties of the NR/WMS–SO_3H composites prevented a readsorption of H_2O produced by the esterification. Furthermore, the mesoporosity and acidity of the NR/WMS–SO_3H catalysts might be a crucial factor in enhancing acid conversion during esterification. Additionally, the NR/WMS–SO_3H catalyst has the potential to be regenerated and reused in the esterification of palmitic acid with methanol.

KEYWORDS: nanocomposite, natural rubber, wormhole-like mesostructured silica, organosulfonic acid, esterification

INTRODUCTION

Esters are essential chemicals used for various applications in chemical industries as they are widely used in manufacturing perfumes, flavors, food products, cosmetics, pharmaceuticals, lubricants, and fuels. The synthesis of organic esters is often achieved by the esterification of carboxylic acids with alcohols using homogenous acid catalysts. However, this process is energy-inefficient and environment-unfriendly owing to the requirement of extensive procedures for product washing and conditioning and treating discharged corrosive wastewater [1–3]. The use of various acid catalysts in the process of esterification has attracted considerable attention due to the catalyst capacity to be reused and the cleanliness of the overall process [4–6]. Furthermore, several acidic substances have been examined as solid catalysts for the process of esterification, which involves the conversion of different carboxylic acids with alcohols. Supported solid acid catalysts can be easily prepared via a simple impregnation method [7, 8]. For example, $H_3PW_{12}O_{40}/Al_2O_3$ is a highly active catalyst used in the esterification of *n*-butanol with simple carboxylic acids [9]. However, it is prone to deactivation by leaching active species, resulting in limited reusability [10].

Bulk catalysts are commonly used as solid acid catalysts, which can be classified into inorganic, organic, and inorganic–organic hybrid/composite materials [11, 12]. The inorganic-based catalysts mainly comprise metal oxides with or without intraparticle porosity such as zeolites, Al-containing mesoporous silica, Nb_2O_5, and aluminosilicate clays [11]. The major advantages of this class of catalysts are high thermal stability and tunable acidity. Furthermore, these catalysts can be regenerated and reused several times. Additionally, their confined porous structure imparts shape-selective properties to these catalysts.

However, the hydrophilicity of the metal-oxide surface results in the readsorption of H_2O, which easily poisons acid sites [11].

The organic-based catalysts include functionalized polymers [13–15] and sulfonated carbons [16–18]. Nafion® is a polymer that contains sulfonic acid groups attached to a polytetrafluoroethylene backbone. Although it possesses strong acid sites and hydrophobicity, the surface area (0.02 m^2/g) and acid content are very low [19]. The Amberlyst® series is widely applied in esterification as a cation-exchange resin with a high content of strong sulfonic acid groups [20–22]. Nevertheless, its actual use is limited due to its poor thermal stability (< 140 °C). In the past decade, sulfonated carbons have received considerable attention in the field of esterification [23, 24]. They can be prepared through the moderate-temperature carbonization of low-cost carbohydrate precursors. However, the subsequent sulfonation under severe acidic conditions is environment unfriendly. Additionally, the number of acid moieties that can be introduced is limited because of the nonporous structure with a very low surface area (< 5.0 m^2/g).

The hybrid/composite-type catalysts incorporate the beneficial properties of inorganic and organic materials. The incorporation of functionalized polymers in these catalysts results in the presence of potent acidic sites and hydrophobic characteristics, while the inclusion of inorganic frameworks contributes to the formation of a porous structure and a substantial surface area in the catalysts. Moreover, composite formation enhances the thermal stability of acidic polymers [25–27]. For example, SAC-13, which is an amorphous silica-supported Nafion® polymer, possesses a large surface area (> 200 m^2/g) and nanometer-scale pore openings (> 10 nm), thereby facilitating its application in the catalytic reaction of bulky reactants. Despite its large application potential, a significant amount of surface silanol groups (≡Si—OH) inhibits the esterification activity in water-sensitive processes [28, 29].

Recently, we successfully prepared propylsulfonic acid-functionalized natural rubber/wormhole-like mesostructured silica (NR/WMS–SO_3H) nanocomposites as a solid acid catalyst for esterification. Compared to other conventional catalysts, NR/WMS–SO_3H exhibited a superior catalytic performance in the esterification of carboxylic acids with ethanol owing to its large surface area, strong acidic moieties, and hydrophobicity, which prevented the readsorption of H_2O on the acid sites [30, 31]. However, this acidic hybrid material has limited application in the esterification of long-chain carboxylic acids owing to a limited pore size (D_p), which renders the diffusion of reactants into the acid sites difficult.

In this study, the effects of the alkyl chain length of primary amines (as templates: $C_nH_{2n+1}NH_2$, n = 12, 14, and 16) on the physicochemical properties of the resulting acidic NR/WMS–SO_3H nanocomposites were systematically investigated considering their mesostructure, mesoporosity, hydrophobicity, and acidity. The catalytic performance of the NR/WMS–SO_3H nanocomposite was compared with that of various propylsulfonic acid-functionalized wormhole-like mesostructured silica (WMS–SO_3H) materials in the esterification of acetic, octanoic, and palmitic acids with methanol. The results of this research will facilitate the development and production of acidic hybrid mesoporous silica catalysts that can be customized in terms of mesoporosity, acidity, and hydrophobicity. These catalysts have potential applications in the esterification of long-chain carboxylic acids.

MATERIALS AND METHODS

Materials

Tetraethyl orthosilicate (TEOS; AR grade 99%), 3-mercaptopropyltrimethoxysilane (MPTMS; AR grade 99%), hydrogen peroxide solution (H_2O_2; AR grade) and primary amines, namely, dodecylamine (C_{12}; AR grade >99%), tetradecylamine (C_{14}; AR grade 95%), and hexadecylamine (C_{16}; AR grade 95%) were purchased from Sigma-Aldrich (USA). Tetrahydrofuran (THF; AR grade 99.5%) was obtained from QREC Chemicals Co. Ltd. (New Zealand). Sulfuric acid (H_2SO_4; AR grade 98%) and absolute ethanol (AR grade 99.5%) were purchased from Merck Millipore Ltd. (Germany). Technically specified NR (standard Thai rubber, grade 5L) was supplied by the Thai Hua Chumporn Natural Rubber Co. Ltd. (Thailand). All materials and reagents were used without further purification.

Synthesis procedure

The NR/WMS–SO_3H nanocomposites were synthesized via *in-situ* sol–gel and co-condensation methods, which were adapted from previous reports, using different primary-amine templates [30–34]. Typically, an NR sheet was first swollen in tetraethyl orthosilicate and then dissolved in tetrahydrofuran under continuous stirring to obtain a homogeneous solution. To the NR solution, a primary amine (dodecylamine, tetradecylamine, or hexadecylamine) was added, followed by a dropwise addition of TEOS. Deionized water, 3-mercaptopropyltrimethoxysilane (MPTMS), and a hydrogen peroxide solution were sequentially added to the mixture, and the resulting gel was stirred at 40 °C for 1 h. The molar gel composition was 0.10 TEOS:0.04 primary amine:5.89 H_2O:0.37 THF:0.01 NR:0.02 MPTMS:0.14 H_2O_2. Finally, the gel was aged at 40 °C for 3 d, after which it was precipitated in 100 ml of ethanol. The obtained white solid was filtered, washed with ethanol, and dried at 100 °C overnight. The organic template was extracted using a solution of 0.05 M H_2SO_4 in ethanol at 70 °C for 4 h. The resulting solid was thoroughly washed with

ethanol until the pH of the filtrate became neutral, followed by drying at 100 °C overnight. The as-prepared acidic mesoporous composite was designated as NR/WMS–C_n–SO_3H, where n represents the number of carbon atoms in the primary amine used.

Additionally, the WMS–SO_3H materials with different primary-amine templates were prepared via the same procedure, in which a molar composition similar to that of NR/WMS–C_n–SO_3H was used but without the NR sheet.

Characterization of WMS–C_n–SO_3H and NR/WMS–C_n–SO_3H

Powder X-ray diffraction (XRD) patterns of the synthesized mesoporous materials were collected at small angles (2θ ranging from 0.5° to 10°) with a scanning step of 0.02° using a Rigaku SmartLab diffractometer (Rigaku Holdings Corporation, Japan) with Cu Kα radiation (λ = 0.154 nm) at 40 kV and 40 mA. The N_2 adsorption–desorption measurement was performed at −196 °C using a Quantachrome Autosorb-1-C chemisorption–physisorption analyzer (Quantachrome Instruments, USA). All the samples (∼ 50 mg) were pretreated in a vacuum at 150 °C for 2 h, and then, their accurate weight was measured prior to adsorption. The specific surface area (S_{BET}) was determined according to the Brunauer–Emmett–Teller (BET) method using adsorption data at relative pressures (P/P_0) of 0.05–0.3. The total pore volume (V_t) was determined using the accumulated N_2 adsorbed volume at a P/P_0 value of approximately 0.99. D_p was calculated via the Barrett–Joyner–Halenda method using the desorption curves of the isotherms.

The material morphologies were studied via scanning electron microscopy (SEM) and transmission electron microscopy (TEM). The SEM images were recorded on a JEOL IT-200 scanning electron microscope (JEOL, Japan) operating at 15 kV. The samples were observed on copper grids without any metal coating. The TEM images were obtained using a JEOL JEM-2010F transmission electron microscope (JEOL) at an accelerating voltage of 200 kV.

Functional groups in these materials were characterized using a Perkin–Elmer Spectrum One Fourier-transform infrared (FTIR) spectrometer (PerkinElmer, USA). The sample wafer was prepared using the KBr method. The FTIR spectra were collected in the transmittance mode between 400 and 4000 cm^{-1}.

The chemical composition of the adsorbent surface was investigated via X-ray photoelectron spectroscopy (XPS) using an ESCA 1700R system (JEOL) with Al Kα1 radiation (1486.8 eV). The C 1s signal at 284.6 eV, corresponding to adventitious carbon, was used to calibrate the binding energy scale. XPS spectra were deconvoluted using the OriginPro 8.5 software before the quantification of different bonding species.

An Elementar Vario Micro Cube CHNS elemental analyzer (Elementar, UK) was used to quantify the amount of sulfur contained in the functionalized materials. The concentration of sulfonic acid groups in the WMS–SO_3H and NR/WMS–SO_3H materials was determined via titration with 0.02 M NaOH using phenolphthalein as an indicator.

H_2O adsorption–desorption analysis was performed to evaluate the hydrophobicity of the WMS–C_n–SO_3H and NR/WMS–C_n–SO_3H nanocomposites. The measurement was performed at 25 °C using a BELSORP-max system (BEL, Japan). Each sample was pretreated similarly as that of N_2 physisorption. The monolayer-adsorbed volume of water (V_m) was obtained from adsorption data at a P/P_0 value of < 0.3.

Esterification of various carboxylic acids with methanol over the WMS–SO_3H and NR/WMS–SO_3H catalysts

The esterification of various carboxylic acids with methanol was performed in a 50 ml stainless autoclave. Before the reaction study, the catalyst was dried at 100 °C for 2 h. The reaction temperatures were set at 80, 100, and 120 °C using an oil bath connected to a thermostat when the acid reactants were acetic, octanoic, and palmitic acids, respectively. In a typical reaction, the operating parameters were as follows: a methanol:carboxylic acid molar ratio of 2:1, catalyst loading of 1 wt% (based on the weight of carboxylic acid used), reaction time of 3 h, and stirring speed of 300 rpm. The reaction mixture was collected at different time intervals and subsequently diluted using THF as solvent. Sample analysis was conducted on a Shimadzu GC-2014 gas chromatograph with a flame ionization detector (Shimadzu, Japan). All reactions were repeated at least twice, and the average initial rate and conversion were reported. The standard deviation was less than 5%. One-way analysis of variance (ANOVA) was used to identify significant variations in the reactant conversion. This was followed by the least significant difference (LSD) test with a significance level of $p < 0.05$. The relationships between the pore diameter and carboxylic acid conversion were analyzed using a simple regression method. Moreover, the thermodynamic equilibrium for the esterification of acetic, octanoic, and palmitic acids with methanol was calculated using the UNIFAC method (vapor–liquid equilibria) employing the ASPEN plus software (version 7.3) [35].

RESULTS AND DISCUSSION

Characterization of the acidic mesoporous catalysts

Fig. 1 shows the XRD patterns of the WMS–SO_3H and NR/WMS–SO_3H materials synthesized using primary-amine templates with different alkyl chain lengths. All the sample patterns exhibited a diffraction peak at 2θ (within the range of 1.0°–3.0°), relating to the charac-

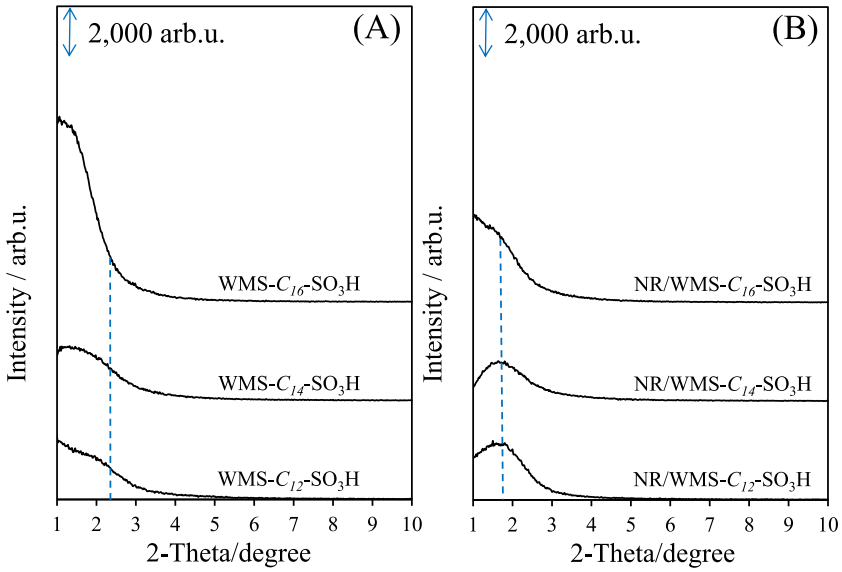

Fig. 1 XRD patterns of the (A) WMS–SO_3H materials and (B) NR/WMS–SO_3H nanocomposites. All samples were extracted to remove the primary amine template prior to the analysis.

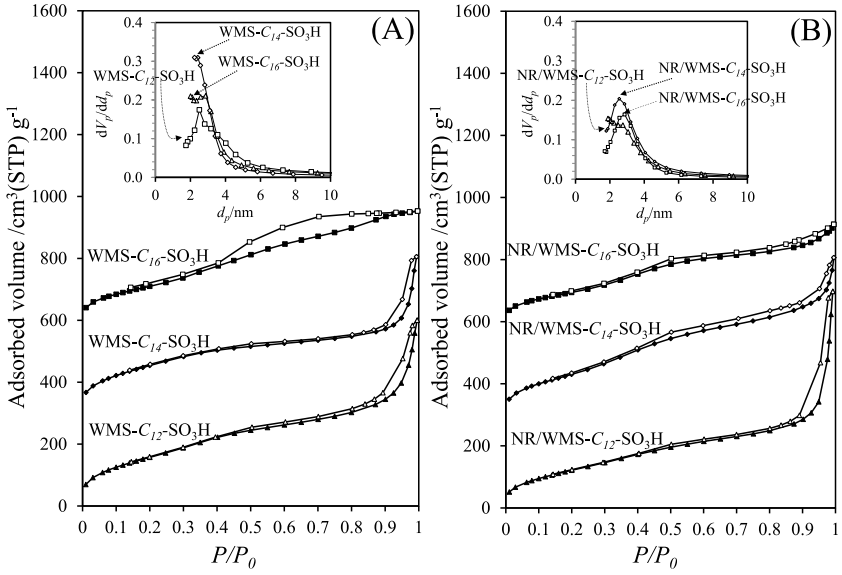

Fig. 2 N_2 adsorption–desorption isotherms and BJH pore size distribution of the (A) WMS–SO_3H materials and (B) NR/WMS–SO_3H nanocomposites. All samples were extracted to remove the primary amine template prior to the analysis.

Table 1 Textural and acid properties of sulfonic acid functionalized WMS and NR/WMS materials.

Sample[a]	S_{BET}[b] (m^2/g)	D_p[c] (nm)	V_t[d] (cm^3/g)	Acid capacity[e] (mmol H^+/g)	Sulfur content[f] (mmol/g)
WMS–C_{12}–SO_3H	596	2.09	0.70	1.23	1.70
WMS–C_{14}–SO_3H	587	2.41	0.54	1.66	1.88
WMS–C_{16}–SO_3H	428	3.17	0.53	1.99	2.27
NR/WMS–C_{12}–SO_3H	506	1.98	0.74	1.07	1.47
NR/WMS–C_{14}–SO_3H	468	2.34	0.62	1.27	1.53
NR/WMS–C_{16}–SO_3H	365	2.86	0.44	1.52	1.59

[a] Extracted samples; [b] BET surface area; [c] Pore diameter, calculated by the BJH method; [d] Total pore volume, determined by the volume adsorbed at $P/P_0 = 0.99$; [e] Determined by acid-base titration with NaOH aq. (0.02 M); and [f] Determined by CHNS analyzer.

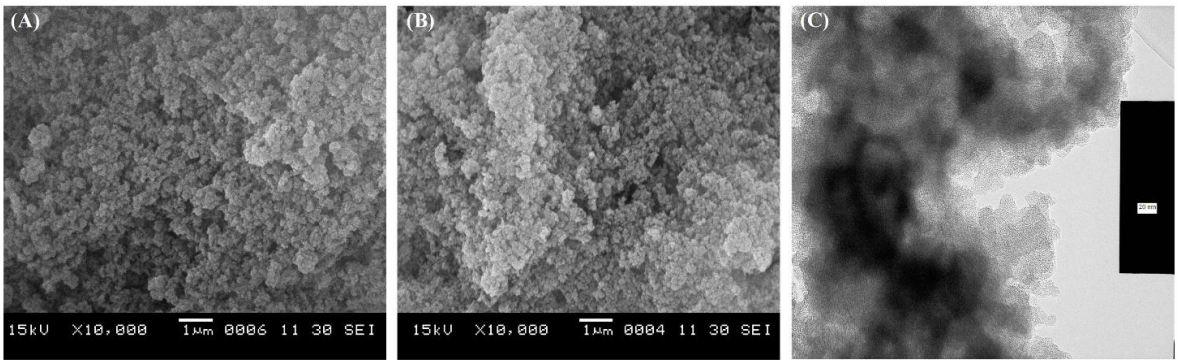

Fig. 3 SEM images (10,000 × magnification) of the (A) WMS–C_{12}–SO_3H, (B) NR/WMS–C_{12}–SO_3H, and (C) TEM image of NR/WMS–C_{12}–SO_3H.

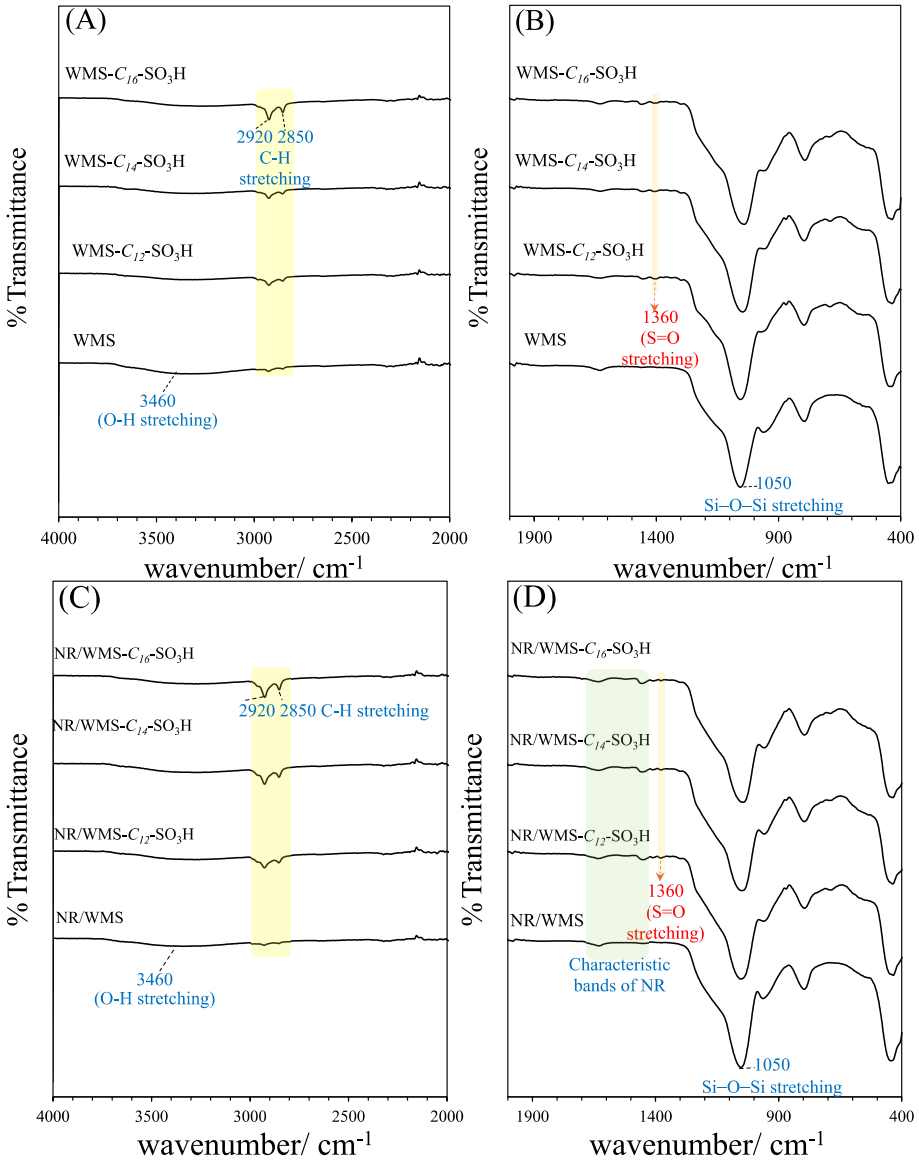

Fig. 4 FTIR spectra of WMS–SO_3H and NR/WMS–SO_3H materials at (A and C) high and (B and D) low energy ranges.

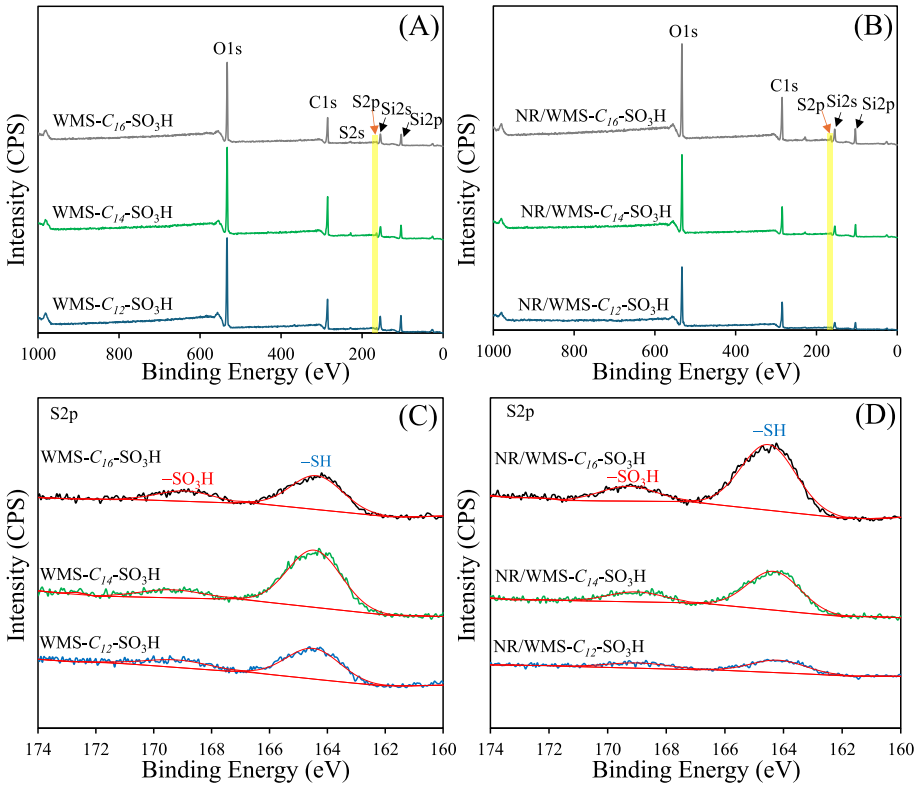

Fig. 5 Representative XPS spectra of WMS–SO_3H and NR/WMS–SO_3H materials showing the (A and B) wide scan spectra and (C and D) high-resolution S 2p region.

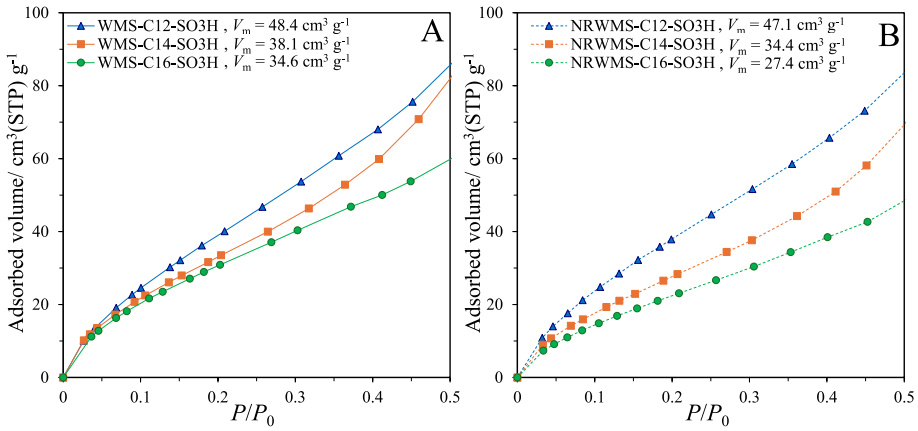

Fig. 6 H_2O adsorption isotherms of the (A) WMS–SO_3H materials and (B) NR/WMS–SO_3H nanocomposites at low relative pressures (P/P_0) in the range of 0–0.5.

teristic (100) plane of the mesoporous material with a wormhole-type pore structure [30]. These results indicate that the materials retained the mesostructure ordering after NR/WMS nanocomposite formation and functionalization. Both materials exhibited a d_{100} diffraction peak that shifted to the lower angle due to the use of longer amine templates for synthesis. This should be attributed to the expansion of the micelle formation. Additionally, the patterns of the functionalized materials synthesized with the longest alkyl-chain template exhibited a highly intense XRD peak. Previous studies have demonstrated that increasing the hydrophobic chain length of template molecules enhances the degree of micelle packing, resulting in a better ordered arrangement [33].

Based on the IUPAC classification, the N_2

adsorption–desorption isotherms of the functionalized WMS and NR/WMS materials were type IV isotherms (Fig. 2), which is a characteristic of framework-confined mesoporous materials. The pore diameters of both the synthesized materials could be systematically controlled using the template chain length (Fig. 2 inset), resulting in an increase in D_p with the template size (Table 1). These results are consistent with the previous work [33], which reported the tuning of wormhole-like mesopores of hexagonal mesoporous silica and natural rubber/hexagonal mesoporous silica nanocomposites in the presence of different primary amine templates. However, the WMS–C_{16}–SO_3H and NR/WMS–C_{16}–SO_3H samples synthesized with the largest amine molecules exhibited lower S_{BET} and V_t values (Table 1). These results agree well with those of previous studies [33, 34] and the reports by Yousatit et al [36]. The mesoporosity decreased because the organic species (propyl sulfonic group and/or NR content) in the WMS silica structure enhanced with the increase of the molecular size of amine-template molecules. Additionally, the mesoporous NR/WMS–SO_3H nanocomposites exhibited lower S_{BET}, D_p, and V_p values than the WMS–SO_3H materials synthesized using the same amine because of the incorporation of NR into the mesoporous silica structure [30]. The FTIR and XPS analyses covered in the next section could confirm these assumptions.

The morphology of the WMS–C_{12}–SO_3H and NR/WMS–C_{12}–SO_3H materials is shown in the representative SEM and TEM images presented in Fig. 3. The SEM image of the NR/WMS–SO_3H nanocomposite exhibited a larger aggregate of nanosized silica particles than WMS–SO_3H. This result indicates that the presence of the rubber phase on the mesosilica structure yields larger particle aggregates and higher interparticle porosity than those in WMS–SO_3H. Additionally, the NR/WMS–SO_3H nanocomposite possessed uniform, framework-confined, mesoporous channels with wormhole-like structures, as revealed by the TEM image.

The qualitative identification of the functional groups is validated through FTIR and XPS spectra shown in Fig. 4 and Fig. 5, respectively. Fig. 4 shows the spectra of the functionalized WMS and NR/WMS materials prepared via the co-condensation method. Bands located at 3100–3700 cm^{-1} in all mesoporous sample spectra (Fig. 4A,C) were due to the O—H stretching vibration of silanol groups and physisorbed H_2O on the mesoporouse silica surface. Bands related to the stretching vibration of the siliceous framework (Si—O—Si) of these samples appeared between 1000 and 1300 cm^{-1}. In the pure silica WMS spectrum (Fig. 4A), weak bands corresponding to C—H vibrations were observed at 2920 and 2850 cm^{-1}. These observations imply that ethoxy groups from the TEOS precursor were not completely hydrolyzed [36]. In the spectra of WMS–SO_3H materials (Fig. 4A,B), bands observed at 1360 (S=O stretching of sulfonic acid groups), 2850, and 2920 cm^{-1} (C—H stretching of methylene groups) were related to propylsulfonic acid groups [37]. The FTIR results also revealed that adding propylsulfonic acid groups to the mesoporous silica surfaces strengthened the peaks associated with C—H stretching compared to the initial WMS.

The presence of NR in the NR/WMS structure (Fig. 4C,D) was deduced from the bands observed at 2920, 2850, 1655, and 1460 cm^{-1}, which corresponded to the NR structure [36]. Additionally, the bands of silanol groups were less pronounced in the NR/WMS spectrum than those in its WMS counterpart, indicating an enhanced hydrophobicity due to the incorporation of the NR phase. Moreover, the spectra of NR/WMS–SO_3H nanocomposites displayed a band related to propylsulfonic acid functionalized onto the surface of NR/WMS at 1360 cm^{-1}.

Fig. 5 shows the XPS spectra of the WMS–SO_3H and NR/WMS–SO_3H materials synthesized using different primary-amine templates. The wide-scan XPS spectra of these materials (Fig. 5A,B) confirmed the presence of sulfur and silica framework structures, exhibiting 6 characteristic bands at 533, 284.5, 233, 160, 151, and 100 eV, corresponding to O 1s, C 1s, S 2s, S 2p, Si 2s, and Si 2p, respectively. The high-resolution S 2p XPS spectrum represented bands corresponding to sulfonic acid species (–SO_3H) at 167–171 eV (Fig. 5C,D). However, the presence of a thiol group (–SH) in these materials was confirmed by the band located between 162–166.5 eV [37]. Bands related to the unoxidized thiol group with H_2O_2 were not detected in the FTIR spectra owing to the weak signal of –SH species [38]. These results indicate that the efficiency of oxidation by H_2O_2 at 40 °C was rather low because the thiol-group oxidation was strongly dependent on temperature. In addition, it is possible that thiol groups were situated in the sublayer of the silica framework, therefore remaining in their unoxidized states [37].

The sulfur content and acidity of the WMS–SO_3H and NR/WMS–SO_3H materials calculated via the CHNS elemental analysis and acid–base titration, respectively, are summarized in Table 1. The acid capacity of these materials was less than the corresponding sulfur content. These results suggest that the oxidation process using H_2O_2 could not convert all the –SH species to the corresponding –SO_3H species. Moreover, with an increase in the template size from C_{12} to C_{16} in the synthesis mixture, the sulfur content and acidity of the resulting materials increased. Probably, the large C_{16} amine could easily introduce MPTMS molecules into mesostructured silica via hydrophobic interactions. Furthermore, the materials prepared using a longer alkyl-chain amine (C_{16}) as

the template displayed a higher degree of micelle packing and a mesostructured silica structure with a larger pore diameter than the materials synthesized with short-chain surfactants (Table 1). These results corroborate well with those of a previous study that demonstrated the tuning of wormhole-like mesopores of WMS and NR/WMS synthesized using different primary-amine templates [33, 34]. Additionally, the conversion of a thiol group to a sulfonic acid group of the NR/WMS–SO_3H series (51%–73%) was lower than that of the WMS–SO_3H materials (53%–85%). These results suggest that several mercaptopropyl groups were embedded in the rubber structure, probably due to a hydrophobic attraction [30].

The H_2O adsorption behavior at low relative pressure was used to evaluate the effects of the incorporation of propylsulfonic acid and/or NR on the hydrophobic properties of WMS–SO_3H and NR/WMS–SO_3H. Fig. 6 shows the H_2O adsorption isotherms of the functionalized materials at P/P_0 values of 0–0.5. In both material series, with increasing template size of the synthesis mixture, the monolayer adsorption volume (V_m) of H_2O decreased, corresponding to a decreased S_{BET} of the resulting materials (Table 1). These results are consistent with previously reported findings that an increase in the number of organic species incorporated into the mesoporous silica structure increases the hydrophobicity of materials [30, 31]. Notably, the NR/WMS–SO_3H composites possessed a higher hydrophobicity than WMS–SO_3H owing to the incorporated NR molecules.

Esterification of various carboxylic acids with methanol

The esterification of carboxylic acids with methanol is an autocatalyzed reaction. Without the addition of catalysts, the esterification of acetic, octanoic, and palmitic acids with methanol spontaneously occurred at 80, 100, and 120 °C, respectively. Equilibrium conversions for the esterification of acetic, octanoic, and palmitic acids at different temperatures without the catalyst addition were calculated via the UNIFAC method as depicted in the Supplementary Information (Fig. S1). The possible acid conversions of these reactions were reported from 80 to 120 °C. Increasing the reaction temperature resulted in a slight decrease in the equilibrium conversion owing to the exothermic characteristics of esterification. The equilibrium conversion of acetic acid at 80 °C, octanoic acid at 100 °C, and palmitic acid at 120 °C was 98.9%, 96.9%, and 93.8%, respectively.

Catalytic study in the esterification of various carboxylic acids with methanol

Fig. 7 shows the initial rates and conversion profiles of acetic and octanoic acids with methanol in the presence of various acidic mesoporous catalysts. The application of acidic solid catalysts to the reaction enhanced the acid conversion. When the WMS–SO_3H and NR/WMS–SO_3H catalysts with increasing pore diameter were applied, initial rates were consistently enhanced, wherein the WMS–C_{16}–SO_3H and NR/WMS–C_{16}–SO_3H catalysts gave the highest initial rate among various catalyst species owing to its high acidity (Fig. 7A). Moreover, the NR/WMS–SO_3H catalysts with a larger number of sulfonic acid groups exhibited a higher initial rate than the NR/WMS–SO_3H catalysts with a similar template size. However, the initial rate observed for octanoic acid was lower than that for acetic acid in esterification with methanol when using both catalysts. This is because the larger molecular size of octanoic acid than that of acetic acid resulted in a slower diffusion into the active sites of these catalysts.

Furthermore, a continuous enhancement of the acetic and octanoic acid conversions is observed when using the WMS–SO_3H and NR/WMS–SO_3H catalysts with increased pore diameters as shown in Fig. 7B. These results indicate that the pore diameter and acid properties of both catalysts affected the reactivity of reactants at the active sites. When using the synthesis mixture of the WMS–SO_3H and NR/WMS–SO_3H catalysts with a similar template size, carboxylic acid conversions observed for both types of catalysts were significantly different, although the NR/WMS–SO_3H catalysts possessed a lower acidity and surface area than the WMS–SO_3H catalysts. This was due to the higher hydrophobicity of the NR/WMS–SO_3H catalysts that caused the deceleration of sulfonic acid–site poisoning or the reduction in the shift of reaction equilibrium toward hydrolysis, as NR could prevent the readsorption of H_2O onto sulfonic acid groups, which was consistent with the previous research [31]. These results are also consistent with the previous work by Chaowamalee et al [37], who reported that the hydrophobicity of propylsulfonic acid groups and natural rubber in mesoporous silica structures could prevent the hydrolysis of alkyl levulinate synthesis. Additionally, the NR/WMS–C_{16}–SO_3H catalyst yielded the highest conversion of acetic (84.1%) and octanoic acids (80.2%) at 3 h (Fig. 7B).

To investigate the advantages of the pore channel of the WMS–SO_3H and NR/WMS–SO_3H catalysts in catalytic esterification, all the acidic mesoporous silica catalysts were comparatively studied in the esterification of palmitic acid with methanol (Fig. 8A). Additionally, the palmitic acid conversions of the WMS–SO_3H and NR/WMS–SO_3H catalysts were plotted against their pore diameters (Fig. 8B) to assess the effects of the mesopore size on catalytic activity. The pore diameter of the acidic mesoporous catalyst is a crucial factor that determines the diffusion of guest molecules. The WMS–C_{16}–SO_3H and NR/WMS–C_{16}–SO_3H catalysts synthesized using the hexadecylamine as the template

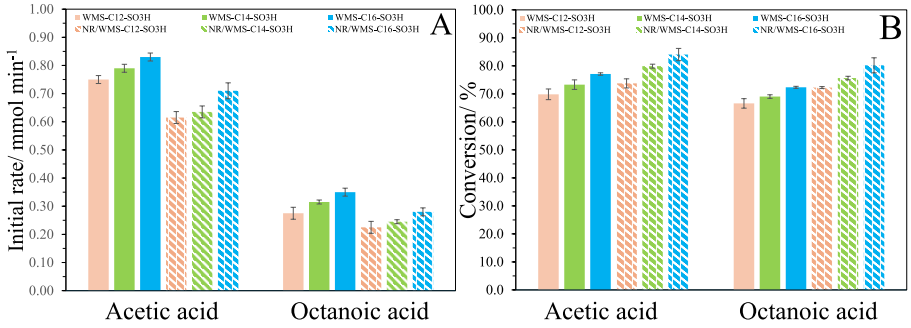

Fig. 7 Esterification of acetic acid and octanoic acid with methanol. (A) Initial rate and (B) conversion of carboxylic acids over WMS–SO_3H and NR/WMS–SO_3H composites. Reaction conditions: catalyst amount, 1 wt%; molar ratio of carboxylic acid:methanol, 1:2; time, 3 h; and temperature, 80 °C and 100 °C when using acetic acid and octanoic acid, respectively.

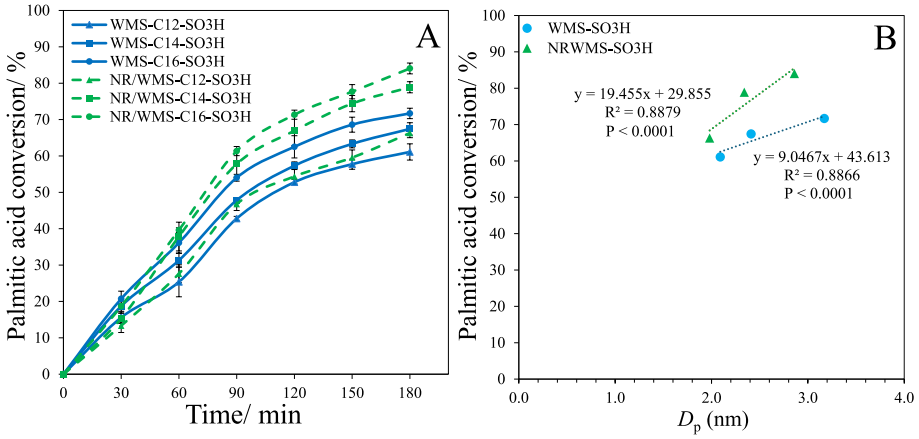

Fig. 8 Esterification of palmitic acid with methanol. (A) Palmitic acid conversion over WMS–SO_3H and NR/WMS–SO_3H composites and (B) relationship of palmitic acid conversion with catalyst pore diameter. Reaction conditions: catalyst amount, 1 wt%; molar ratio of palmitic acid:methanol, 1:2; time, 3 h; and temperature, 120 °C.

exhibited the highest palmitic acid conversion (71.7% and 84.1%, respectively). This result was similar to that reported by Qian et al [39], who observed an enhanced catalytic activity of a metal–organic framework catalyst with an enlarged pore structure for fatty acid methyl ester production.

Moreover, the NR/WMS–SO_3H catalysts exhibited a higher acid conversion than the WMS–SO_3H catalysts, although the former possessed a lower acidity and surface area than the latter. This was due to the higher hydrophobicity of the NR/WMS–SO_3H catalysts than that of the other tested catalysts, which promoted the diffusion of the long hydrocarbon chain molecules such as palmitic acid molecules to the acid sites. Additionally, the effect of hydrophobicity in conjunction with D_p on conversion was deduced from the superior performance of the NR/WMS–C_{16}–SO_3H catalyst compared to that of other tested catalysts, depicting the highest conversion of palmitic acid. The mechanistic pathways of the esterification of palmitic acid with methanol over the NR/WMS–SO_3H composites are postulated in Supplementary Information (Fig. S2). These results revealed that the NR/WMS–SO_3H catalyst with enhanced hydrophobicity and pore diameter was advantageous for the esterification of carboxylic acids with long hydrocarbon chains.

Reusability of the NR/WMS–SO_3H composite in esterification

The reusability of the NR/WMS–C_{16}–SO_3H catalyst was preliminarily evaluated in the esterification of palmitic acid with methanol under suitable reaction conditions. The spent NR/WMS–C_{16}–SO_3H catalyst was recovered from the reaction mixture via filtration, followed by thorough washing with acetone and overnight drying at 100 °C. As shown in Supplementary Information (Fig. S3A), the catalyst can be repeatedly used at least 5 times in esterification, during which the palmitic acid conversion gradually decreased to 79%.

After the esterification of palmitic acid, the spent NR/WMS–C_{16}–SO_3H catalyst was analyzed using FTIR spectroscopy, N2 physisorption measurements, and CHNS elemental analysis to investigate the stability of the organic moieties incorporated in its mesoporous

structure (Fig. S3B). The FTIR spectra of spent catalysts obtained after washing with acetone were similar to those of fresh catalysts. This result revealed that acetone was a good solvent for removing the reaction mixture from the surface of the NR/WMS–SO_3H catalyst. However, the spent catalysts showed a lower SBET than the fresh catalyst. Additionally, CHNS elemental analysis revealed that the spent catalyst had a slightly lesser S content than the fresh catalyst. These results indicated that a small amount of palmitic acid and/or the ester product remained adhered on the catalyst surface.

CONCLUSION

The NR/WMS–SO_3H catalysts with diverse mesoporosity, acidity, and hydrophobicity were successfully prepared via an *in-situ* sol–gel technique using C_{12}–C_{16} primary amines as templates. They were applied as hybrid/composite acid catalysts in the esterification of various carboxylic acids with methanol. The effects of the different types of the amine template on the mesostructure and textural properties of the NR/WMS–SO_3H nanocomposites were similar to those of the WMS–SO_3H series; however, the presence of NR reduced the structural ordering and mesoporosity. Increasing the molecular size of amine-template molecules increased the pore diameter and acidity of the NR/WMS–SO_3H series. The NR molecules dispersed in the mesoporous silica framework created a hydrophobic environment in the NR/WMS–SO_3H catalysts. Here, the acid sites located in the mesoporous channels were less poisoned by H_2O generated from esterification compared with those in the WMS–SO_3H catalysts. Furthermore, the enhanced pore-channel structure and acidity of the NR/WMS–SO_3H catalysts promoted the initial reaction rate and acid conversion, particularly in the esterification of long hydrocarbon chain carboxylic acids such as octanoic and palmitic acids with methanol. Additionally, with the highest pore diameter and acidity, the NR/WMS–C_{16}–SO_3H catalyst could be reused at least 5 times in the esterification of palmitic acid in the presence of methanol. Meanwhile, the acid conversion was maintained at approximately 79%. Moreover, the presence of a cumulated carboxylic acid and/or ester product on the surface was assumed to be caused by the deactivation of the NR/WMS–SO_3H catalyst. Therefore, the NR/WMS–SO_3H catalyst is a potential solid acid catalyst for biodiesel production.

Appendix A. Supplementary data

Supplementary data associated with this article can be found at https://dx.doi.org/10.2306/scienceasia1513-1874.2024.s002.

Acknowledgements: The authors are grateful to the financial support from the Thailand Science Research and Innovation (TSRI), annual government statement B.E. 2566–2567, Fundamental Fund (Project code 181350). The financial support from the Thailand Research Fund (TRF) under the International Research Network: Functional Porous Materials for Catalysis and Adsorption (Grant no. IRN61W0003) is acknowledged. The authors also acknowledge the technical support from the Center of Excellence in Catalysis for Bioenergy and Renewable Chemicals (CBRC), and Center of Excellence on Petrochemical and Materials Technology (PETROMAT), Chulalongkorn University.

REFERENCES

1. Liu Y, Lotero E, Goodwin J (2006) A comparison of the esterification of acetic acid with methanol using heterogeneous versus homogeneous acid catalysis. *J Catal* **242**, 278–286.
2. Bala DD, Misra M, Chidambaram D (2017) Solid-acid catalyzed biodiesel production, part I: biodiesel synthesis from low quality feedstock. *J Clean Prod* **142**, 4169–4177.
3. Loures C, Amaral M, Da Rós P, Elerbrock Zorn S, Castro H, Silva M (2017) Simultaneous esterification and transesterification of microbial oil from *Chlorella minutissima* by acid catalysis route: A comparison between homogeneous and heterogeneous catalysts. *Fuel* **211**, 261–268.
4. Li M, Chen J, Huang Y, Li M, Lin X, Qiu T (2020) Reusable and efficient heterogeneous catalysts for biodiesel production from free fatty acids and oils: Self-solidifying hybrid ionic liquids. *Energy* **211**, 118631.
5. Yu Z, Chen X, Zhang Y, Tu H, Pan P, Li S, Han Y, Piao M, et al (2022) Phosphotungstic acid and propylsulfonic acid bifunctionalized ordered mesoporous silica: A highly efficient and reusable catalysts for esterification of oleic acid. *J Chem Eng* **430**, 133059.
6. Kurniawan YS, Thomas K, Hendra, Jumina, Wahyuningsih TD (2021) Green synthesis of alkyl 8-(2-butyl-5-octyl-1, 3-dioxolan-4-yl)octanoate derivatives as potential biolubricants from used frying oil. *ScienceAsia* **47**, 64–71.
7. Morales M, Infantes-Molina A, Lázaro Martínez J, Romanelli G, Pizzio L, Rodriguez-Castellon E (2020) Heterogeneous acid catalysts prepared by immobilization of $H_3PW_{12}O_{40}$ on silica through impregnation and inclusion, applied to the synthesis of 3H-1, 5-benzodiazepines. *Mol Catal* **485**, 110842.
8. Buchori L, Widayat W, Hadiyanto H, Satriadi H, Chasanah N, Kurniawan MR (2022) Modification of magnetic nanoparticle lipase catalyst with impregnation of Activated Carbon Oxide (ACO) in biodiesel production from PFAD (Palm Fatty Acid Distillate). *Bioresour Technol* **19**, 101137.
9. Sharma Dr P, Vyas S, Patel A (2004) Heteropolyacid supported onto neutral alumina: Characterization and esterification of 1° and 2° alcohol. *J Mol Catal A Chem* **214**, 281–286.
10. Zhu S, Zhu Y, Gao X, Mo T, Zhu Y, Li Y (2013) Production of bioadditives from glycerol esterification over zirconia supported heteropolyacids. *Bioresour Technol* **130**, 45–51.
11. Okuhara T (2002) Water-tolerant solid acid catalysts. *Chem Rev* **102**, 3641–3666.
12. Sirsam R, Hansora D, Usmani G (2016) A mini-review on solid acid catalysts for esterification reactions. *J Inst Eng (India) E* **97**, 167.

13. Caetano CS, Guerreiro L, Fonseca IM, Ramos AM, Vital J, Castanheiro JE (2009) Esterification of fatty acids to biodiesel over polymers with sulfonic acid groups. *Appl Catal* **359**, 41–46.
14. Pan Y, Alam MA, Wang Z, Wu J, Zhang Y, Yuan Z (2016) Enhanced esterification of oleic acid and methanol by deep eutectic solvent assisted Amberlyst heterogeneous catalyst. *Bioresour Technol* **220**, 543–548.
15. Wolska J, Stawicka K, Walkowiak-Kulikowska J (2021) Sulfonic-acid-functionalized polymers based on fluorinated methylstyrenes and styrene as promising heterogeneous catalysts for esterification. *Mater Chem Phys* **273**, 125132.
16. Ngaosuwan K, Goodwin Jr JG, Praserthdam P (2016) A green sulfonated carbon-based catalyst derived from coffee residue for esterification. *Renew Energy* **86**, 262–269.
17. Huang L, Song C, Yingcen L, Lin H, Ye W, Huang H, Lu R, Zhang S (2021) Enhancement of catalytic esterification by tuning molecular diffusion in sulfonated carbon. *Microporous Mesoporous Mater* **318**, 111024.
18. Sangsiri P, Laosiripojana N, Daorattanachai P (2022) Synthesis of sulfonated carbon-based catalysts from organosolv lignin and methanesulfonic acid: Its activity toward esterification of stearic acid. *Renew Energy* **193**, 113–127.
19. Martínez F, Morales G, Martín A, Grieken R van (2008) Perfluorinated Nafion-modified SBA-15 materials for catalytic acylation of anisole. *Appl Catal* **347**, 169–178.
20. Park JY, Kim DK, Lee JS (2010) Esterification of free fatty acids using water-tolerable Amberlyst as a heterogeneous catalyst. *Bioresour Technol* **101S1**, 62–65.
21. Pappu VK, Kanyi V, Santhanakrishnan A, Lira CT, Miller DJ (2013) Butyric acid esterification kinetics over Amberlyst solid acid catalysts: the effect of alcohol carbon chain length. *Bioresour Technol* **130**, 793–797.
22. Gee JC, Fulbright KW (2023) Competitive double bond isomerization and competitive esterification of C8 to C18 linear 1-alkenes on amberlyst®15 catalyst: Calculation of relative adsorption coefficients in two concurrent reactions. *Appl Catal* **663**, 119307.
23. Cao M, Peng L, Xie Q, Xing K, Lu M, Ji J (2021) Sulfonated Sargassum horneri carbon as solid acid catalyst to produce biodiesel via esterification. *Bioresource Technology* **324**, 124614.
24. Pan H, Sun J, Liu J, Zhang Y, Zhou S (2021) Preparation of sulfonated carbon derived from orange peel and its application in esterification. *Chem Phys Lett* **770**, 138395.
25. Helminen J, Paatero E (2006) Inorganic solid supported polymer acid catalyst–Sulfonated polystyrene grafted silica gel in liquid phase esterification. *React Funct Polym* **66**, 1021–1032.
26. Zhang X, Lei Z, Yang Q (2014) Designed synthesis of sulfonated polystyrene/mesoporous silica hollow nanospheres as efficient solid acid catalysts. *J Mater Chem A* **2**, 7546–7554.
27. Shestakova P, Popova M, Szegedi Á, Lazarova H, Nga Luong TK, Trendafilova I, Mihály J, Parac-Vogt TN (2021) Hybrid catalyst with combined Lewis and Brønsted acidity based on ZrIV substituted polyoxometalate grafted on mesoporous MCM-41 silica for esterification of renewable levulinic acid. *Microporous Mesoporous Mater* **323**, 111203.
28. Ledneczki I, Darányi M, Fulop F, Molnar A (2005) SAC-13 silica nanocomposite solid acid catalyst in organic synthesis. *Catal Today* **100**, 437-440.
29. Climent MJ, Corma A, Iborra S, Martínez-Silvestre S, Velty A (2013) Preparation of glycerol carbonate esters by using hybrid Nafion-silica catalyst. *ChemSusChem* **6**, 1224–1234.
30. Nuntang S, Poompradub S, Butnark S, Yokoi T, Tatsumi T, Ngamcharussrivichai C (2014) Organosulfonic acid-functionalized mesoporous composites based on natural rubber and hexagonal mesoporous silica. *Mater Chem Phys* **147**, 583–593.
31. Nuntang S, Yokoi T, Tatsumi T, Ngamcharussrivichai C (2016) Enhanced esterification of carboxylic acids with ethanol using propylsulfonic acid-functionalized natural rubber/hexagonal mesoporous silica nanocomposites. *Catal Commun* **80**, 5–9.
32. Nuntang S, Yousatit S, Chaowamalee S, Yokoi T, Tatsumi T, Ngamcharussrivichai C (2017) Mesostructured natural rubber/*in situ* formed silica nanocomposites: A simple way to prepare mesoporous silica with hydrophobic properties. *Microporous Mesoporous Mater* **259**, 79–88.
33. Nuntang S, Yousatit S, Yokoi T, Ngamcharussrivichai C (2019) Tunable mesoporosity and hydrophobicity of natural rubber/hexagonal mesoporous silica nanocomposites. *Microporous Mesoporous Mater* **275**, 235–243
34. Jermjun K, Khumho R, Thongoiam M, Yousatit S, Yokoi T, Ngamcharussrivichai C, Nuntang S (2023) Natural rubber/hexagonal mesoporous silica nanocomposites as efficient adsorbents for the selective adsorption of (–)-epigallocatechin gallate and caffeine from green tea. *Molecules* **28**, 6019.
35. Calvar N, González B, Dominguez A (2007) Esterification of acetic acid with ethanol: Reaction kinetics and operation in a packed bed reactive distillation column. *Chem Eng Process Process Intensif* **46**, 1317–1323.
36. Yousatit S, Rungruangwattanachot W, Yuwawanitchakorn N, Nuntang S, Punyapalakul P, Ngamcharussrivichai C (2023) Amine-functionalized natural rubber/mesostructured silica nanocomposites for adsorptive removal of clofibric acid in aqueous phase. *Molecules* **28**, 2330.
37. Chaowamalee S, Yan N, Ngamcharussrivichai C (2022) Propylsulfonic acid-functionalized mesostructured natural rubber/silica nanocomposites as promising hydrophobic solid catalysts for alkyl levulinate synthesis. *Nanomater* **12**, 604.
38. Cano-Serrano E, Campos-Martin JM, Fierro JLG (2003) Sulfonic acid-functionalized silica through quantitative oxidation of thiol groups. *Chem Comm* **2003**, 246–247.
39. Qian L, Cheng J, Xin K, Guo H, Mao Y, Tu J, Yang W (2023) Enhancing catalytic activity and pore structure of metal–organic framework-808 via ligand competition for biodiesel production from microalgal lipids at reduced temperatures. *Bioresour Technol* **386**, 129533.

Appendix A. Supplementary data

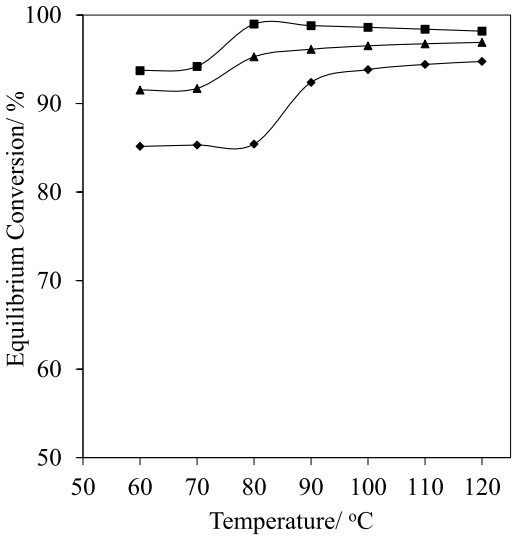

Fig. S1 Equilibrium conversion of esterification of (—■—) acetic acid, (—▲—) octanoic acid, and (–◆–) palmitic acid with methanol at different temperatures as calculated by UNIFAC method.

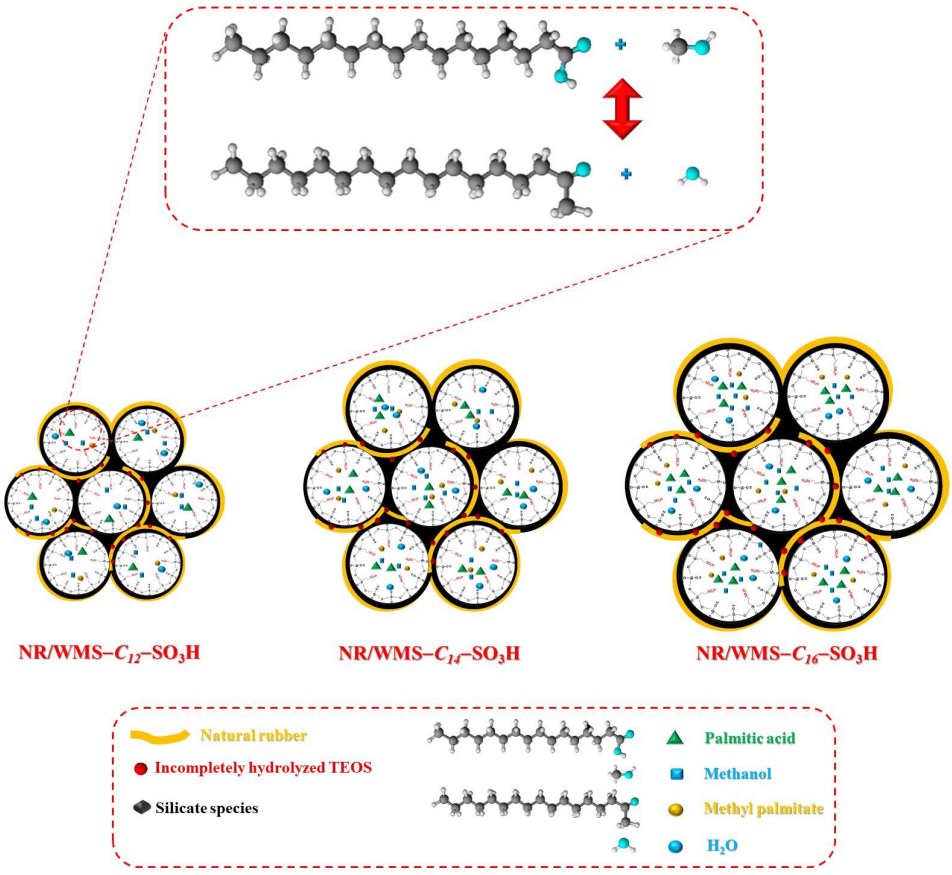

Fig. S2 Plausible mechanistic pathways of the esterification of palmitic acid with methanol over NR/WMS–SO_3H composites.

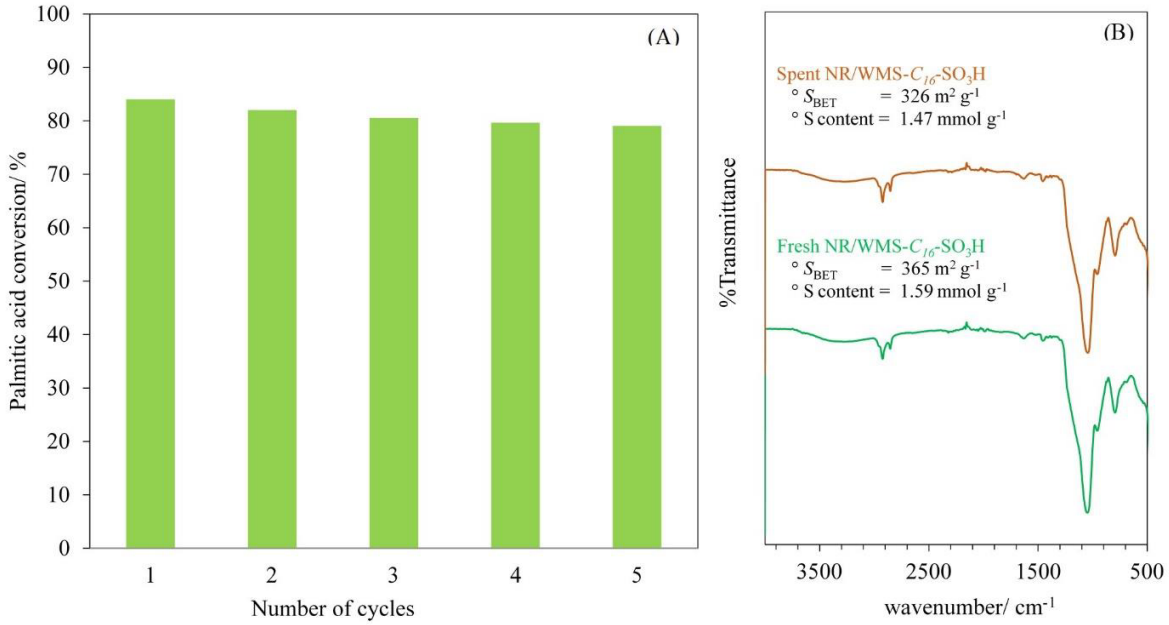

Fig. S3 Reusability of NR/WMS–C_{16}–SO_3H in esterification of palmitic acid with methanol. Reaction conditions: catalyst amount, 1 wt%; molar ratio of palmitic acid:methanol, 1:2; time, 3 h; and temperature, 120 °C.